Institutions of the Russian Academy of Sciences
Joint Institute for High Temperatures RAS
Institute of Problems of Chemical Physics RAS
Kabardino-Balkarian State University

Physics of Extreme States of Matter — 2010

Chernogolovka, 2010

Physics of Extreme States of Matter — 2010

Edited by academician Fortov V. E., Karamurzov B. S., Temrokov A. I., Efremov V. P., Khishchenko K. V., Sultanov V. G., Levashov P. R., Kanel G. I., Iosilevski I. L., Milyavskiy V. V., Mintsev V. B., Petrov O. F., Savintsev A. P., Shpatakovskaya G. V.

This compendium is devoted to investigations in the fields of thermal physics of extreme states of matter and physics of high energy densities. Different models and results of theoretical calculations of equations of state of matter at high pressure and temperature, physics of shock and detonation waves, experimental methods of diagnostics of ultrafast processes, interaction of intense laser, x-ray and microwave radiation, powerful ion and electron beams with matter, techniques of intense energy fluxes generation, low-temperature plasma physics, issues of physics and power engineering, and technology projects are considered. The majority of the works has been presented at the XXV International Conference on Equations of State for Matter (March 1–6, 2010, Elbrus, Kabardino-Balkaria, Russia). The edition is intended for specialists in physical and technical problems of power engineering.

The conference is sponsored by the Russian Academy of Sciences and the Russian Foundation for Basic Research (grant No. 10-02-06043).

ISBN 978-5-901675-96-0

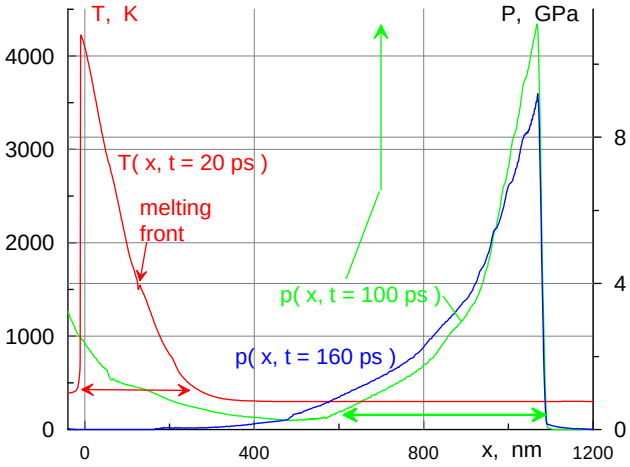

Figure 4. Extension of the pressure profile due to nonlinear reflection at the glass-Al boundary. The pressure profile is longer than the temperature profile which produces the pressure profile—compare the horizontal arrows.

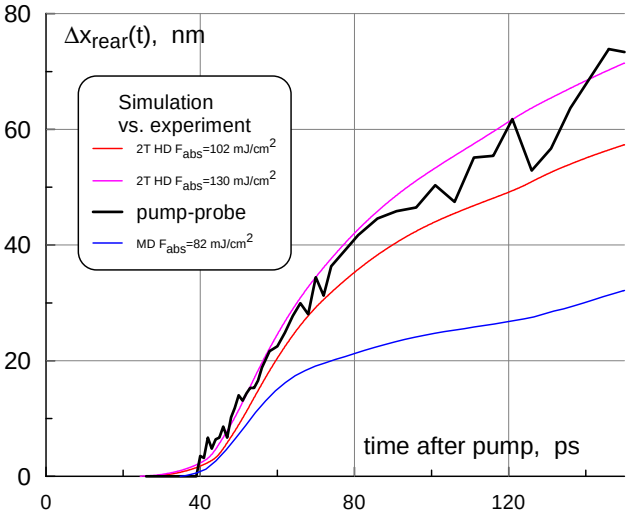

Figure 5. Transformation of pressure profile into time dependence of the shift Δx_{rear}. The Al foil thickness is 350 nm, $\tau_L = 150$fs. The F_{abs} in simulation is adjusted to fit the experimental data.

The nonlinear reflection of the minus wave at the glass-Al boundary greatly extends the width of the acoustic wave propagating to the right side. The pump-probe measurements detect this extension. The extended pressure profiles are shown in Fig. 4. The full width of the $p(x, t = 100\text{ps})$ profile is 470 nm, whereas the width of the T-profile is ≈ 270nm at the instant $t = 20$ps. At this instant the characteristic starting from the point $x = 0, t = 0$ crosses the d_T-layer, see Fig. 3. The width of the T-profile gives the width of the plus pressure wave without the tail. The two widths of the $T(x, t = 20\text{ps})$ and $p(x, t = 100\text{ps})$ are marked by the horizontal arrows.

The amplitude of the pressure tail is a measure of temperature of Al at the glass-Al boundary after e-i relaxation. In its turn, this temperature is linked to the 2T electron heat conductivity κ : since higher κ corresponds to lower temperatures. Comparison of two profiles at $t = 100$ and 160 ps is shown in Fig. 4. The profile $t = 100$ps is shifted to the position of the $p(x, t = 160\text{ps})$ profile. The maximum of the profile $t = 100$ps before the shift is marked by the vertical arrow.

Comparison of calculated and measured shift profiles is shown in Fig. 5.

Conclusions. In summary, we find two new acoustic phenomena caused by thermomechanical response to UsLP irradiation. They are the imprint of 2T supersonic melting into acoustic signal and formation of a tail due to nonlinear interaction of acoustic and entropy modes. We show that the model [5] for 2T κ describes experimental data.

The work has been supported by the RFBR grant No. 09–08–00969-a.

1. N.A. Inogamov, V.V. Zhakhovskii, S.I. Ashitkov et al., Appl. Surf. Sci. **255,** (2009) 9712; arXiv:0812.2965v1[physics.optics].
2. Wai-Lun Chan, R. S. Averback, D. G. Cahill, A. Lagoutchev, Phys. Rev. **B 78,** (2008) 214107.
3. S. Amoruso, R. Bruzzese, X. Wang et al., J. Phys. D: Appl. Phys. **40,** (2007) 331.
4. Z. Lin, L.V. Zhigilei, V. Celli, Phys. Rev. **B 77,** (2008) 075133.
5. N. A. Inogamov, Yu. V. Petrov, JETP **137,** (2010) No. 2 (in press).
6. V. V. Zhakhovskii, N. A. Inogamov et al., Appl. Surf. Sci. **255,** 9592 (2009).
7. A. V. Bushman, G. I. Kanel', A. L. Ni, V. E. Fortov, Intense dynamic loading of condensed matter, (Taylor & Francis Translation, 1993) 295 p. http://teos.ficp.ac.ru/rusbank/
8. D.J. Funk, D.S. Moore, S.D. McGrane, K.T. Gahagan et al., Thin Solid Films **453–454,** (2004) 542.
9. L. Huang, Y. Yang, Y. Wang, Z. Zheng, W. Su, J. Phys. D: Appl. Phys. **42,** (2009) 045502.

ELECTRON COLLISION FREQUENCY AND HEAT CONDUCTIVITY OF SIMPLE METALS UP TO THE ELECTRON TEMPERATURES COMPARED WITH THE FERMI TEMPERATURE

Petrov Yu. V.**, Inogamov N.A.

ITP RAS, Chernogolovka, Russia

**uvp49@mail.ru*

Introduction. When operating with two-temperature hydrodynamics equations one needs the values of parameters characterizing the target material in this state such as the electron-ion energy relaxation coefficient α_{ei}, electron heat capacity c_e, electron heat conductivity κ_e. . It is often used the phenomenological models the electron heat conductivity κ_e is presented as the combination of low temperature asymptotic value and high temperature plasma expression with taking into account the limiting value of the

electron collision frequency. Low temperature (when the electron temperature T_e and Fermi temperature T_F obey the relationship $T_e \ll T_F$) asymptotic value of the electron collision frequency is presented then in the form of a sum of electron-ion and electron-electron frequencies: $\nu_e = AT_i + BT_e^2$. The coefficient A in the electron-ion part ν_{ei} of the electron collision frequency is experimentally defined with a sufficient accuracy both for solid and liquid state of aluminum in the temperature range from temperature up to 2–3 kK. For higher temperatures in a liquid state there is a quantum mechanics calculation together with the molecular dynamics simulation [1]up to $T_e = T_i = 10kK$. At the same time the value of a coefficient B in the electron-electron part ν_{ee} of full electron collision frequency is not defined so well. Theoretical estimations [2, 3]give even various values of the B order. We have calculated electron-electron collision frequency ν_{ee} of simple metals up to moderate electron temperatures of the order of Fermi temperature T_F as distinct from other calculations restricted by low electron temperatures.

Electron collision frequency. The frequency of collisions of the chosen electron with the wave vector $\vec{k}_1$ can be written in the form of the sum over wave vectors of the second electron $\vec{k}_2$ and transferred wave vector $\vec{q}$ [2–4]

$$\nu_{ee}(k_1) = (2\pi/\hbar)\sum_{\vec{k}_2}\sum_{\vec{q}}[U(\vec{q})]^2\delta(\epsilon_1+\epsilon_2-\epsilon_1'-\epsilon_2')S. \quad (1)$$

Here $\vec{q} = \vec{k}_1' - \vec{k}_1 = \vec{k}_2 - \vec{k}_2'$ with wave vectors of the chosen electron and the second electron after collision $\vec{k}_1'$ and $\vec{k}_2'$ We consider conduction electrons in a simple metal with the isotropic parabolic dispersion within the effective mass m approach

$$\epsilon(\vec{k}) = \gamma k^2, \quad \gamma = \hbar^2/2m.$$

Thus function $\nu_{ee}(\vec{k}_1)$ (1) depends upon only $k_1 \equiv |\vec{k}_1|$. Delta-function in (1) stands for the energy conservation low, S is a statistical factor

$$S = f_2(1-f_1')(1-f_2') + f_1'f_2'(1-f_2), \quad (2)$$

$$f_1 \equiv f(\epsilon_1), \quad f_1' \equiv f(\epsilon_1'), \quad f_2 \equiv f(\epsilon_2), \quad f_2' \equiv f(\epsilon_2'),$$

$$f(\epsilon) = \left(1+\exp\left(\frac{\epsilon-\mu}{T_e}\right)\right)^{-1}$$

with $f(\epsilon)$ being Fermi distribution function, $\mu(T_e)$ is a chemical potential.

$$U(q) = 4\pi e^2/(q^2+k_s^2) \quad (3)$$

is a Fourrier transformation of the screened Coulomn interaction between two electrons with reverse screen length k_s [2–4].

Expression (1) can be written as a six-dimensional integral over $d^3q/(2\pi)^3\, 2d^3k_2/(2\pi)^3$ Writing d^3q and d^3k_2 in spherical coordinates

$$d^3q = q^2\, dq\, d\psi_q\, dt, \quad t = -\cos\widehat{k_1q},$$

$$d^3k_2 = k_2^2\, dk_2\, d\psi_{k2} dt_2, \quad t_2 = -\cos\widehat{qk_2}.$$

and introducing the transferred energy

$$\alpha = \epsilon_1 - \epsilon_1', \quad \beta = \epsilon_2' - \epsilon_2, \quad (4)$$

$$\alpha = \gamma k_1^2 - \gamma(\vec{k}_1+\vec{q})^2 = 2\gamma q k_1 t - \gamma q^2,$$

$$\beta = \gamma(\vec{k}_2-\vec{q})^2 - \gamma k_2^2 = 2\gamma q k_2 t_2 + \gamma q^2,$$

one can present the integrand in the form

$$U^2(q)\delta(\alpha-\beta)S \quad (5)$$

with

$$S = f(k_2)[1-f(\gamma k_1^2-\alpha) - f(\gamma k_2^2+\beta)] + f(\gamma k_1^2-\alpha)f(\gamma k_2^2+\beta). \quad (6)$$

Because of independence of itegrand (5,6) on the azimuth angles ψ_{k2} and $d\psi_q$, we can write

$$\int\int\int\int\int\int ...d^3q\, d^3k_2 = \int\int\int\int ...2\pi\, q^2\, dq\, dt\, 2\pi\, k_2^2\, dk_2\, dt_2. \quad (7)$$

Taking into account definition (4) we obtain

$$d\alpha = 2\gamma\, q\, k_1\, dt, \quad d\beta = 2\gamma\, q\, k_2\, dt_2. \quad (8)$$

and

$$2\pi\, k_2^2\, dk_2\, dt_2 = \frac{\pi}{\gamma}\frac{k_2}{q} dk_2\, d\beta,$$

$$2\pi\, q^2\, dq\, dt = \frac{\pi}{\gamma}\frac{q}{k_1} dq\, d\alpha.$$

Now the collision frequency for the electron with given wave number k_1 takes the form

$$\nu_{ee}(k_1) = \frac{1}{2(2\pi)^3\hbar\gamma^2}\int\int\int\int U^2(q)\delta(\alpha-\beta)S(k_1,k_2,\alpha,\beta)\frac{k_2}{k_1} dq\, dk_2\, d\alpha\, d\beta, \quad (9)$$

with S given by the expression (6). Delta-function $\delta(\alpha-\beta)$ reduces the integration over β to

$$\nu_{ee}(k_1) = \{1/[2(2\pi)^3\hbar\gamma^2 k_1]\}\times \int\int\int U^2(q)S(k_1,k_2,\alpha,\alpha)k_2 dq\, dk_2\, d\alpha, \quad (10)$$

where the statistical factor can be easily integrated over α in analytic functions:

$$\int S d\alpha = T_e\frac{e^{\epsilon_1/T_e}+e^{\mu/T_e}}{e^{\epsilon_2/T_e}+e^{\mu/T_e}}\frac{e^{(\epsilon_2+\mu)/T_e}}{e^{2\mu/T_e}-e^{(\epsilon_1+\epsilon_2)/T_e}}\times \ln\frac{e^{\epsilon_1/T_e}+e^{(\alpha+\mu)/T_e}}{e^{(\alpha+\epsilon_2)/T_e}+e^{\mu/T_e}} = T_e\frac{1+e^{(\epsilon_1-\mu)/T_e}}{1+e^{(\epsilon_2-\mu)/T_e}}\times \frac{e^{(\epsilon_2-\mu)/T_e}}{1-e^{(\epsilon_1+\epsilon_2-2\mu)/T_e}}\ln\frac{e^{(\epsilon_1-\mu)/T_e}+e^{\alpha/T_e}}{1+e^{(\alpha+\epsilon_2-\mu)/T_e}} = s(\epsilon_2,\alpha;\epsilon_1,\mu,T_e) = s(\alpha). \quad (11)$$

With t, t_2 changed within the range $[-1, 1]$. we have the boundaries for β and α:

$$[\beta' = \gamma(q^2 - 2k_2 q)] \le \beta \le [\beta'' = \gamma(q^2 + 2k_2 q)] \quad (12)$$

$$[\alpha' = -\gamma(2k_1 q + q^2)] \le \alpha \le [\alpha'' = \gamma(2k_1 q - q^2)]. \quad (13)$$

Then limits of integration in the equation (11) are obtained from the condition $\beta' < \alpha < \beta''$ giving four contributions into $\nu_{ee}(k_1)$:

$$\nu_{ee}(k_1)/\xi = I_a + I_b + I_c + I_d, \qquad \xi = 1/[2(2\pi)^3 \hbar \gamma^2 k_1]. \quad (14)$$

Here

$$I_a = I_{a1} + I_{a2} \quad (15)$$

$$I_{a1} = \int_0^{k1} dq \int_{k2=-q+k1}^{k2=q+k1} dk_2\, U^2\, k_2\, [s(\alpha'') - s(\beta')], \quad (16)$$

$$I_{a2} = \int_{k1}^{\infty} dq \int_{k2=q-k1}^{k2=q+k1} dk_2\, U^2\, k_2\, [s(\alpha'') - s(\beta')]$$

$$I_b = \int_0^{\infty} dq \int_{k2=q+k1}^{\infty} dk_2\, U^2\, k_2\, [s(\alpha'') - s(\alpha')] \quad (17)$$

$$I_c = 0,$$

$$I_d = \int_0^{k_1} dq \int_0^{k2=-q+k1} dk_2\, U^2\, k_2\, [s(\beta'') - s(\beta')]. \quad (18)$$

Heat conductivity. From the kinetic equation for the electron distribution function within the τ-approach [2, 3]

$$\vec{v}(\partial f/\partial \vec{r}) = \vec{v}(\partial f/\partial T)\nabla T_e = -f^{(1)}/\tau. \quad (19)$$

where $f(\epsilon)$ is a Fermi distribution function (2) we can obtain $f^{(1)}$, the change of the equilibrium electron distribution due to the temperature gradient, and then a heat flow

$$\vec{Q} = \int (\epsilon - \mu)\, \vec{v}\, f^{(1)}\, \frac{2d^3k}{(2\pi)^3}, \quad (20)$$

It gives the heat conductivity coefficient

$$\kappa_{ee} = \frac{k_B}{3} \int (\epsilon - \mu)\, (-f'_\epsilon)\, [\mu'_T + (\epsilon - \mu)/T_e\,] \times v^2\, \tau(\epsilon)\, \frac{k^2 dk}{\pi^2}, \quad (21)$$

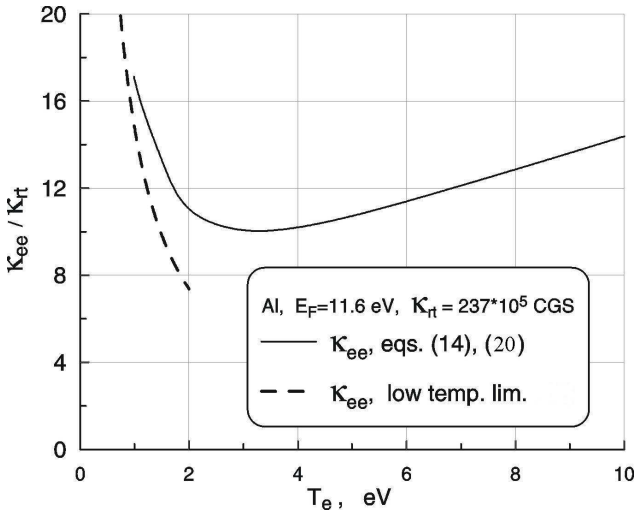

Figure 1. Electron heat conductivity of aluminum due to the electron-electron collisions normalized to the experimental room temperature value.

where $v = v(k) = \hbar k/m$ is the electron velocity. Expression (21) is applicable to single-band metals. This approach is sufficient for aluminum up to electron temperatures of about several tens eV because of the wide energy interval between conduction and inner shell electrons. For the gold with its d-band overlap with s-p-band the validity of this single-band approximation is restricted by essentially lower electron temperatures $T_e \sim 1$ eV. Heat conductivity coefficient of aluminum as a function of the electron temperature is shown in Fig. 1. At low temperatures κ_{ee} tends to the asymptotic behavior $\kappa_{ee} \sim T_e^{-1}$. The range of the applicability of low temperature asymptotic expression is small compared with T_F ($\sim 10\%$ of T_F). At $T_e = 1$ eV the low temperature value of κ is 15% smaller than the value calculated from (21).

We can define then the effective frequency of electron-electron collisions ν_{ee} according to the Drude

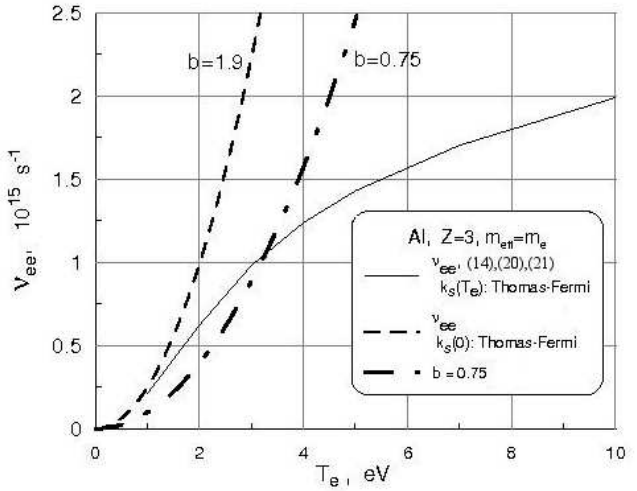

Figure 2. Effective electron-electron collision frequency derived from the electron heat conductivity coefficient of aluminum (solid line) together with its low temperature asimptotics (b=3.8, parabolic dashed line) and another parabola with b=1.5.

formula for heat conductivity to obtain

$$\nu_{ee} = \nu_{ee}|_\kappa = c_{eV}\,\overline{v^2}/(3\kappa_{ee}), \qquad (22)$$

where c_{eV} is the electron heat capacity per the unit volume, $\overline{v^2}$ is a temperature dependent mean squared electron velocity. At low temperatures, when $\nu_{ee} \propto T_e^2$, it can be written as

$$\nu_{ee}|_{lT} = b\,(E_F/\hbar)\,(k_B\,T_e/E_F)^2. \qquad (23)$$

The effective frequency ν_{ee} as a function of the electron temperature is shown in Fig. 2 together with the low temperature asymptotic behavior (equation (23), $b = 3.8$).

Fig.2 also shows that the temperature range for the applicability of low temperature asymptotics of the collision frequency is restricted by the temperatures essentially smaller than the Fermi temperature. When using calculations based upon the equations (14), (22), at higher temperatures the dependence of the electron-electron collision frequency on the electron temperature differs to a great extent from the parabolic function.

Due to the wide change of the electron temperature we used in our calculations Thomas-Fermi screening of the electron-electron interactions with the reverse screening length

$$k_s = \sqrt{\frac{4\pi e^2}{(\partial\mu/\partial n)_T}}$$

and chemical potential dependent both on the temperature and density n of electrons. Thus the screening length in our case at given density depends on the electron temperature and decreases with temperature increase.

1. Recoules V., Crocombette J.-P. // Phys. Rev. B 2005. V. 72. P. 104202.
2. Abrikosov A. A. Introduction to the theory of metals. M.: Nauka, 1987 [in Russian].
3. Ashcroft N. W. , Mermin N. D. Solid State Physics. Saunders College, New York.: Holt, Rinehart and Winston, 1976.
4. Gasparov V. A., Huguenin R. // Advances in Physics. 1993. V. 42. P. 393.

OPTIMIZATION OF K_α YIELD FROM THE TARGET COVERED WITH SPHERICAL CLUSTERS IRRADIATED BY FEMTOSECOND LASER PULSE

Kostenko O.F.*, Andreev N.E.

JIHT RAS, Moscow, Russia

**olegkost@ihed.ras.ru*

Introduction. Experimental study of hard x-ray production from intense short pulse laser irradiation of solid targets coated with dielectric spheres of well-defined sizes exhibited a peak in K_α yield when the spheres with diameter roughly half the laser wavelength were employed [1]. This effect was attributed to electric field enhancement at the surface of the particle and multipass stochastic heating of fast electrons. We present the model for calculations of K_α yield taking into account accelerating field depletion due to laser power absorption by fast electrons, heated according to Brunel mechanism [2] at the surface of perfectly conducting sphere, which imitates metal or overdense plasma cluster. Such approach is analogous to the method applied in Ref. [2] for consideration of the flat target.

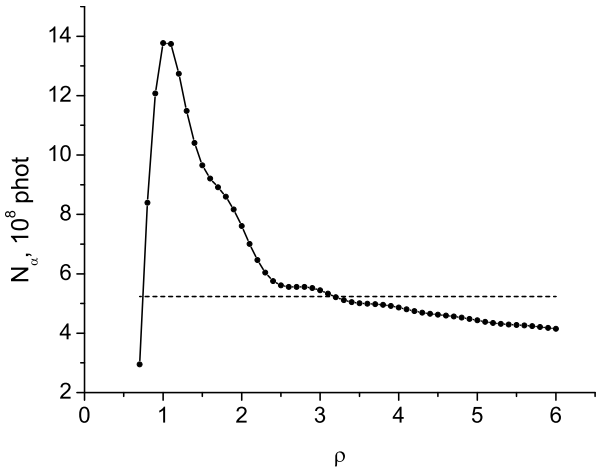

Figure 1. The K_α yield from the copper substrate vs ρ. Dashed line—the K_α yield from the copper solid (cf. Ref. [5]). $I_L = 2 \times 10^{17}$ W/cm^2, $\theta = 45°$. Laser wave-length $\lambda = 0.4$ μm, $r_0 = 5$ μm, laser pulse duration $\tau_p = 40$ fs.

Model. Electric field outside the cluster is a superposition of the incident laser field and the field of a scattered wave, $\mathbf{E} = \mathbf{E}_i + \mathbf{E}_s$. The latter is described by real reflection coefficient, $\mathbf{E}_s = r\mathbf{E}_{s0}$, with $\mathbf{E}_{s0}$ being the electric field of the wave scattered by the perfectly conducting sphere. If the field $\mathbf{E}_i$ is the field of a plane wave that is polarized in the x direction and propagates along the z axis, $\mathbf{E}_i = \mathbf{e}_x E_L \exp(ik_0 z - i\omega t)$, then the radial component of electric field $\mathbf{E}$ at the cluster surface is given by

$$E_0(r,\rho,\theta_1,\varphi_1) = -E_L e^{-i\omega t}\frac{\cos\varphi_1}{\rho}\sum_{n=1}^{\infty} i^{n+1}(2n+1) \times P_n^1(\cos\theta_1)\left[j_n(\rho) + r b_n^r h_n^{(1)}(\rho)\right]. \qquad (1)$$

Here, $\rho = k_0 R$, with R being the cluster radius; $j_n(\rho)$ and $h_n^{(1)}(\rho)$ are spherical Bessel functions of the first and third kinds, and $P_n^1(\cos\theta_1)$ is the associated Legendre function. In spherical coordinates, the angle θ_1 is measured from the direction of the wave vector $\mathbf{k}_0 \| \mathbf{e}_z$ and the angle φ_1, from the direction of the polarization vector $\mathbf{e}_x$. Coefficients of the expansion of the field $\mathbf{E}_{s0}$ in solenoidal vector spherical wave functions for the case of the sphere's permittivity $\epsilon \to -\infty$ are